WSRC-TR-2001-00391

KEYWORDS:
Sludge Suspension
Computational Approach
CFD Approach
Jet Flow Model
Mixing Pump Model
RETENTION - Permanent

PERFORMANCE ANALYSIS FOR MIXING PUMPS IN TANK 18

SAVANNAH RIVER TECHNOLOGY CENTER

Si Young Lee and Richard A. Dimenna

October 2001

Westinghouse Savannah River Company
Savannah River Site
Aiken, SC 29808

SAFETY • RESPONSIBILITY • SECURITY
SRS
SAVANNAH RIVER SITE

Prepared for the U.S. Department of Energy under Contract No. DE-AC09-96SR18500

This document was prepared in conjunction with work accomplished under Contract No. DE-AC09-96SR18500 with the U.S. Department of Energy.

DOCUMENT: **WSRC-TR-2001-00391**
TITLE: **Performance Analysis for Mixing Pumps in Tank 18**

APPROVALS

____ Date:____________
Si Y. Lee, Author (EM&S Group/ SRTC)

____ Date:____________
Richard A. Dimenna, Co-Author (EM&S Group/ SRTC)

____ Date:____________
Robert A. Leishear, Technical Reviewer (WRC Engineering)

____ Date:____________
Cynthia P. Holding-Smith, Manager (EM&S Group/SRTC)

____ Date:____________
Steve T. Wach, Manager (EDS/SRTC)

(This Page Intentionally Left Blank)

Table of Contents

(This Page Intentionally Left Blank)

List of Figures

List of Tables

Nomenclature

A = area (ft^2 or m^2)

d = nozzle diameter (ft or m)

D = tank diameter (ft or m)

C = constant or interpolation factor (--)

F = Force (N)

g = gravity (m/sec^2)

h = liquid height above the nozzle (inch)

H = total tank level (inch)

I = turbulence intensity (--)

k = turbulent kinetic energy (= $\frac{1}{2}\left(u'^2+v'^2+w'^2\right)_{avg}$)

P = pressure (Pa)

Pr = Prandtl number, $\mu C_p/k$, (--)

r = radial distance from the center of tank center (ft or m)

R = tank radius (ft or m)

Re = Reynolds number, $d\rho u/\mu$

t = time (second)

U = nozzle exit velocity (ft/sec or m/sec)

u = component velocity in x-direction (ft/sec or m/sec)

u' = local turbulent velocity fluctuation in x-direction (ft/sec or m/sec)

v = local flow velocity or component velocity in y-direction (ft/sec or m/sec)

v' = local turbulent velocity fluctuation in y-direction (ft/sec or m/sec)

V = average velocity magnitude (ft/sec or m/sec)

w = component velocity in z-direction (ft/sec or m/sec)

w' = local turbulent velocity fluctuation in z-direction (ft/sec or m/sec)

x = local position along the x-direction under Cartesian coordinate system (ft or m)

y = local position along the y-direction under Cartesian coordinate system (ft or m)

z = local position along the y-direction under Cartesian coordinate system (ft or m)

Greek

ρ = density (kg/m^3)

ε = rate of dissipation of turbulent kinetic energy

∇ = gradient operator

Ω = vorticity

ψ = solid weight per weight of liquid

μ = dynamic viscosity (N sec/m^2)

ν = kinematic viscosity (m^2/sec)

η = non-dimensional distance (--)

ϕ = ratio of local velocity to velocity at nozzle exit (--)

Subscript

avg = average

f = fluid

fo = clear fluid

fs = suspended fluid

L = lifting

m = maximum

o = jet nozzle exit

p = particle or pump

s = static

t = turbulent flow

v = flow velocity or vertical

μ = viscosity

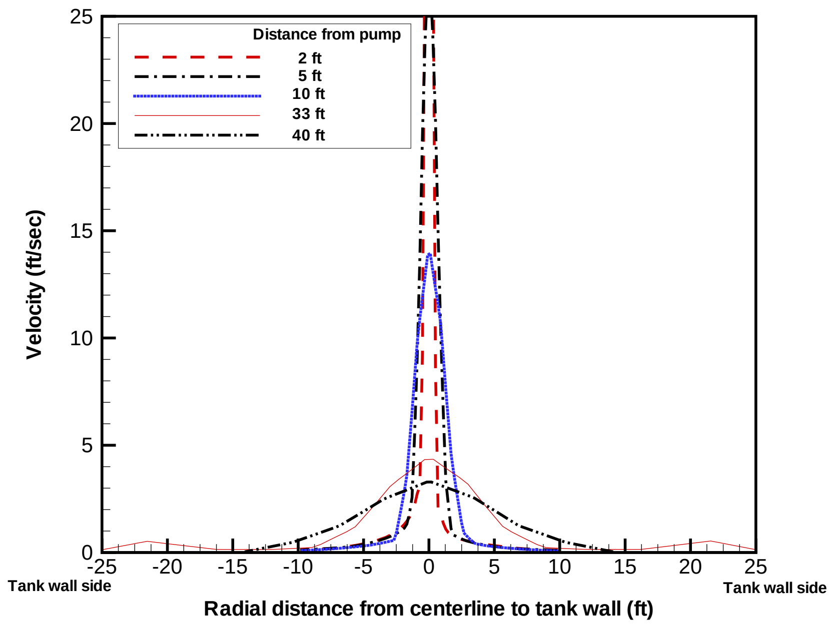

Figure 18. Steady-state horizontal velocity profiles for various distances from the pump at the nozzle discharge plane (27 inches above tank bottom): 3D Model Results for the Full Tank 18 Facility with 70" liquid level

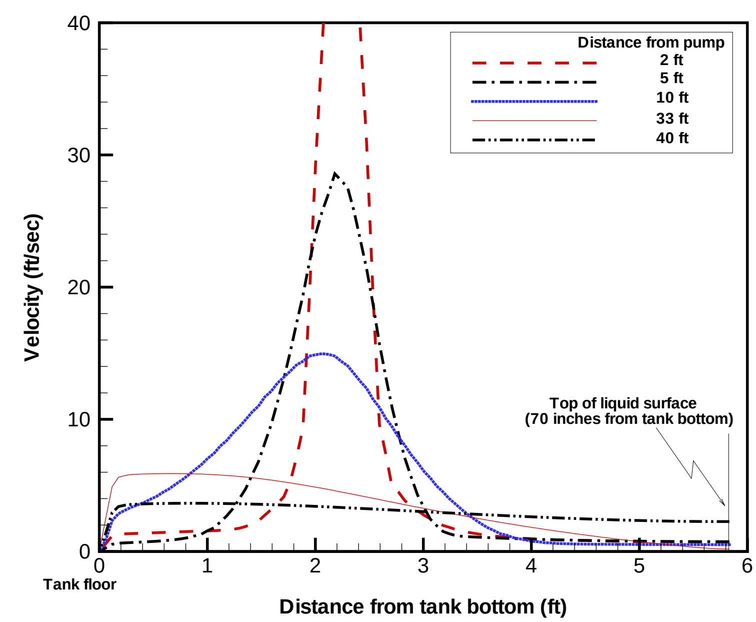

Figure 19. Steady-state vertical velocity profiles for various distances from the pump (pump nozzle is located 2.25ft from tank bottom): 3D Model Results for the Full Tank 18 Facility with 70" liquid level

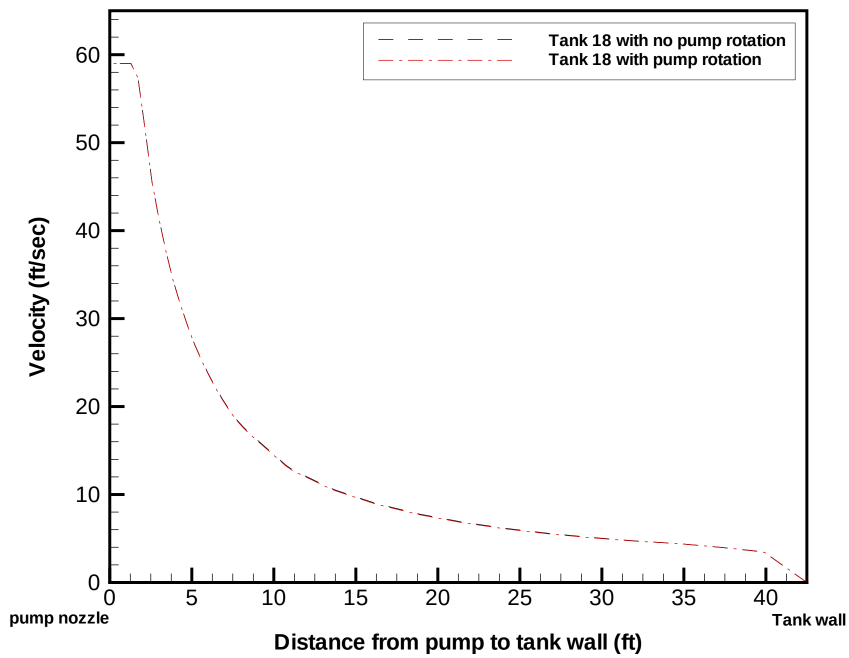

Figure 20. Downstream evolutions of Tank 18 with and without pump rotations for 70 in tank level at the discharge plane 27 inches above the tank bottom.

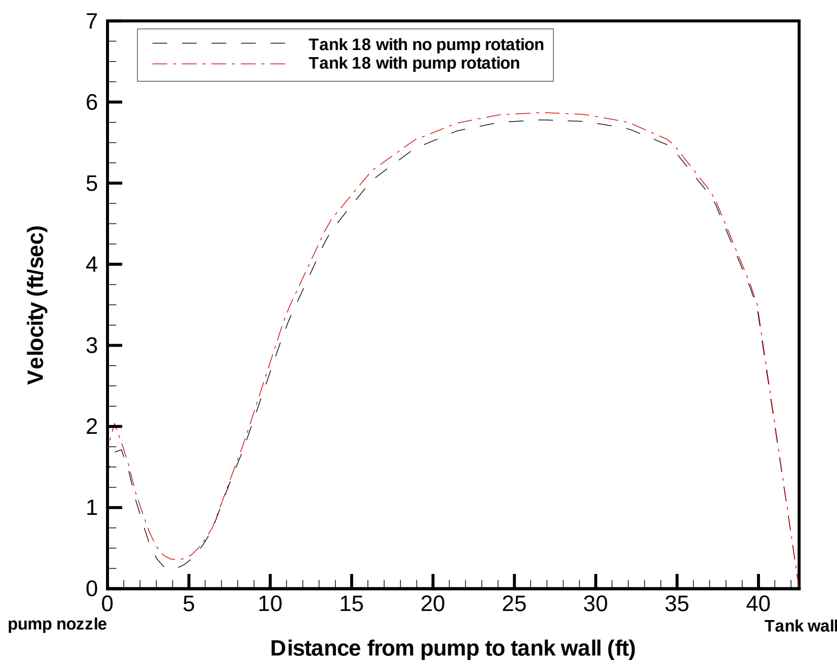

Figure 21. Downstream evolutions of Tank 18 with and without pump rotations for 70 in tank level at the plane 3 inches above the tank bottom.

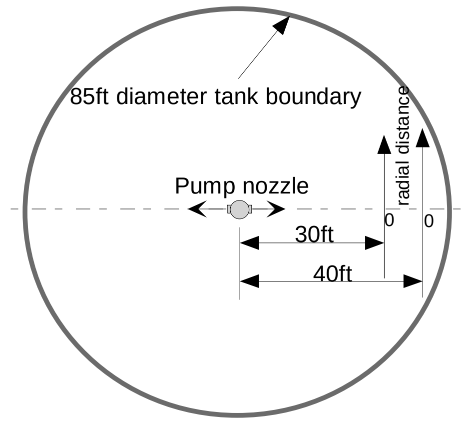

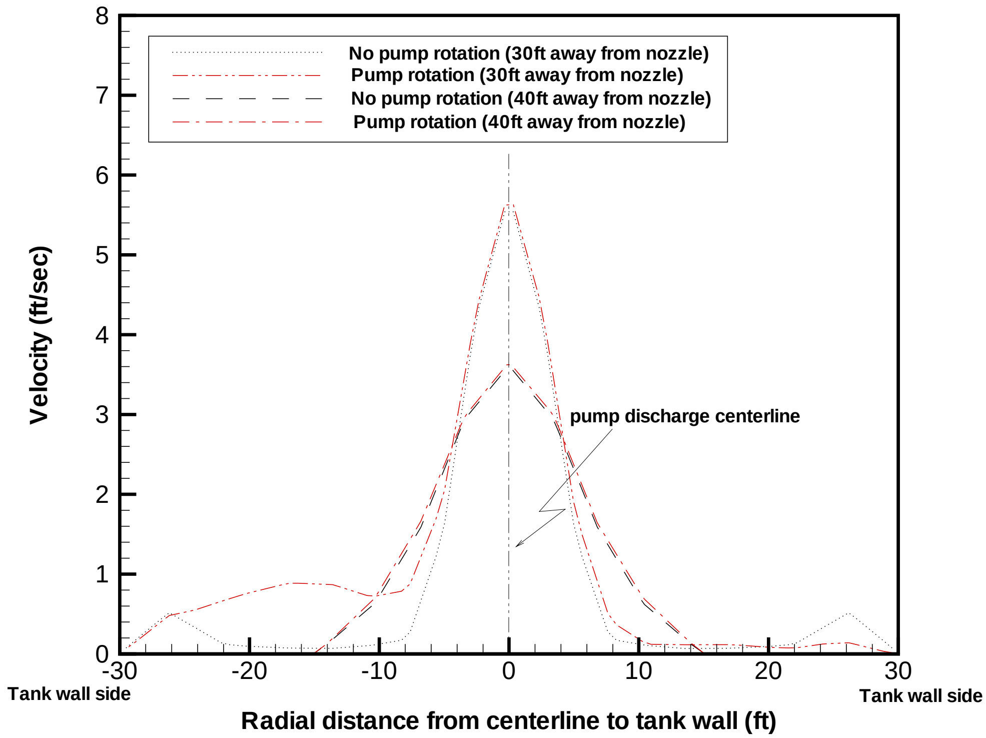

Figure 22. Comparison of steady-state velocity profiles near the wall regions about 12ft and 2ft away from the side wall of Tank 18 at the plane 3 in above tank bottom

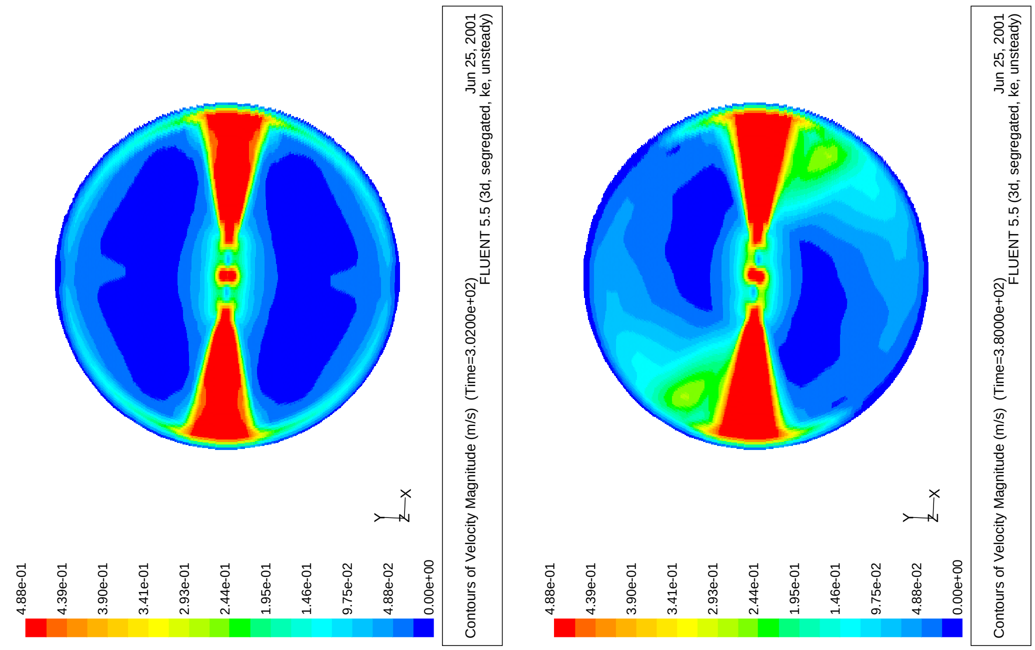

(Flow patterns for no pump rotation) (Flow patterns for pump rotation)

Figure 23. Comparison of steady-state flow patterns of the 3 in plane for Tank 18 without pump rotation and with pump rotation (The red zone is higher than 1.6 ft/sec of flow velocty.)

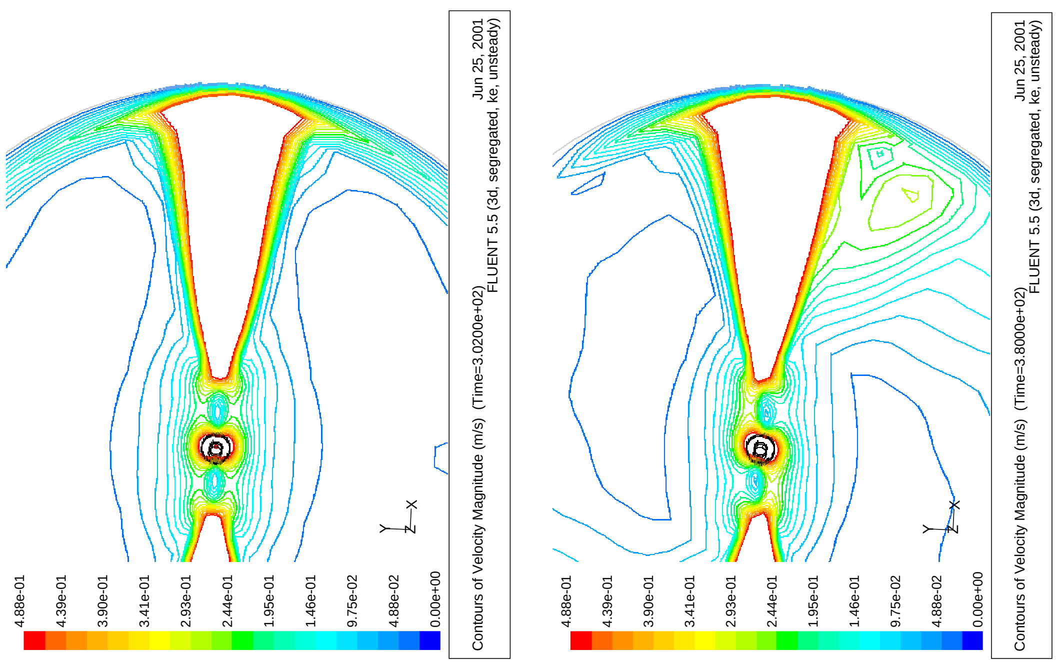

(Near-wall flow pattern for no pump rotation) (Near-wall flow pattern for pump rotation)

Figure 24. Comparison of steady-state velocity contour plots for Tank 18 without pump rotation and with pump rotation at the plane 3 in above the tank bottom (The zone inside the red curve is higher than 1.6 ft/sec of flow velocity.)

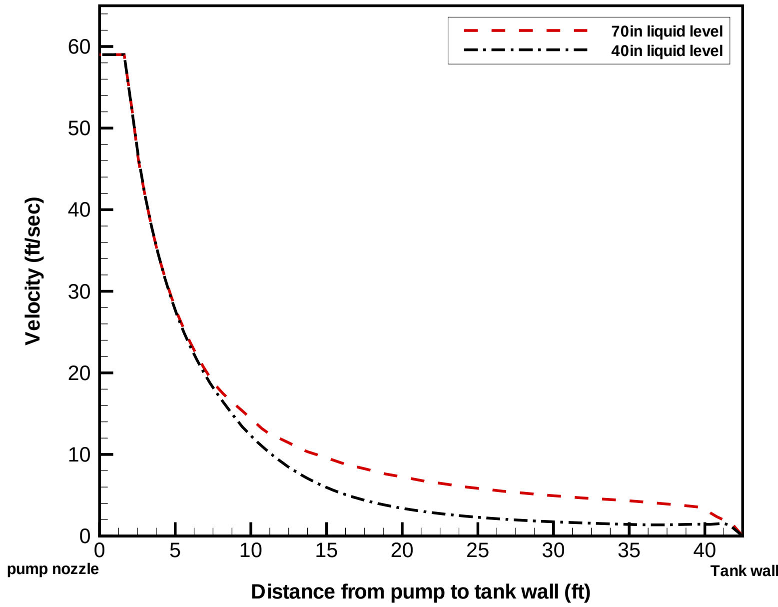

Figure 25. Velocity profiles for various distances from the pump at the nozzle discharge plane (27 inches above tank bottom)

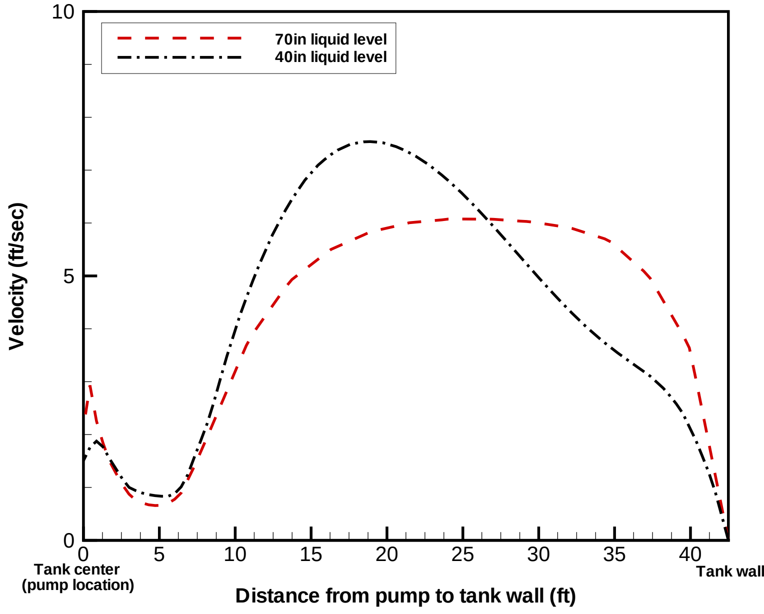

Figure 26. Velocity profiles for various distances from the pump at the nozzle discharge plane (3 inches above tank bottom)

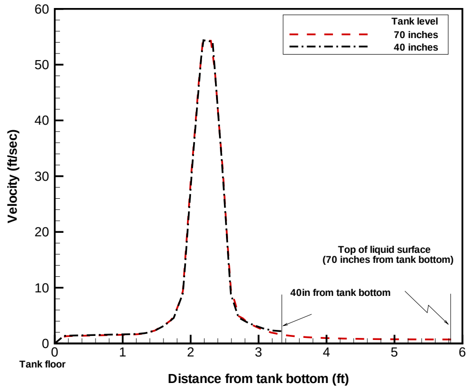

(2 ft from the pump)

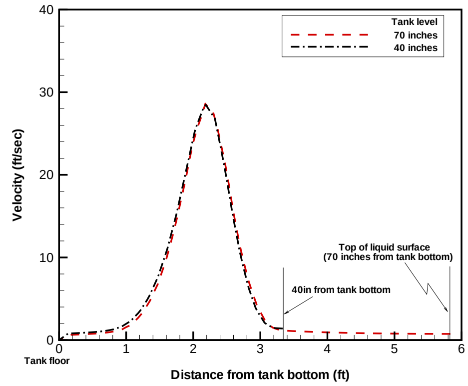

(5 ft from the pump)

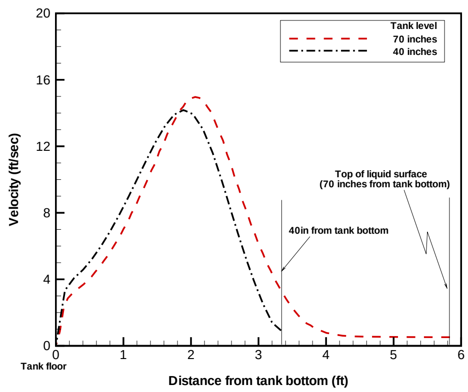

(10 ft from the pump)

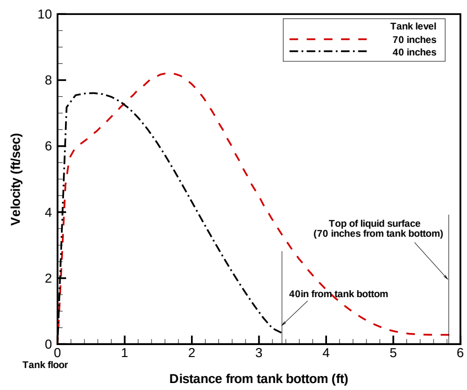

(20 ft from the pump)

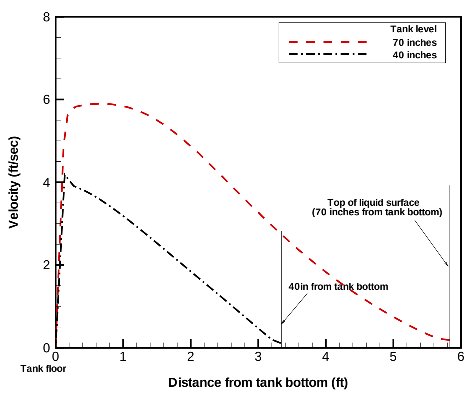

(33 ft from the pump)

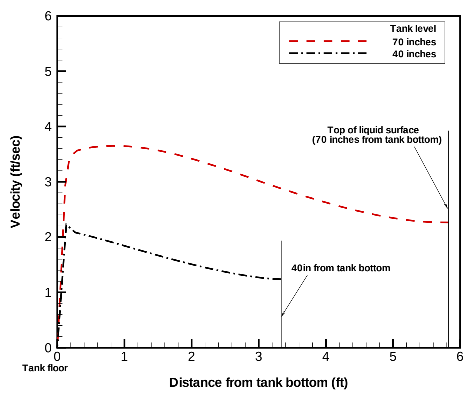

(40 ft from the pump)

Figure 27. Vertical velocity profiles of two different tank levels for various distances from the pump (pump nozzle is located 2.25ft from tank bottom)

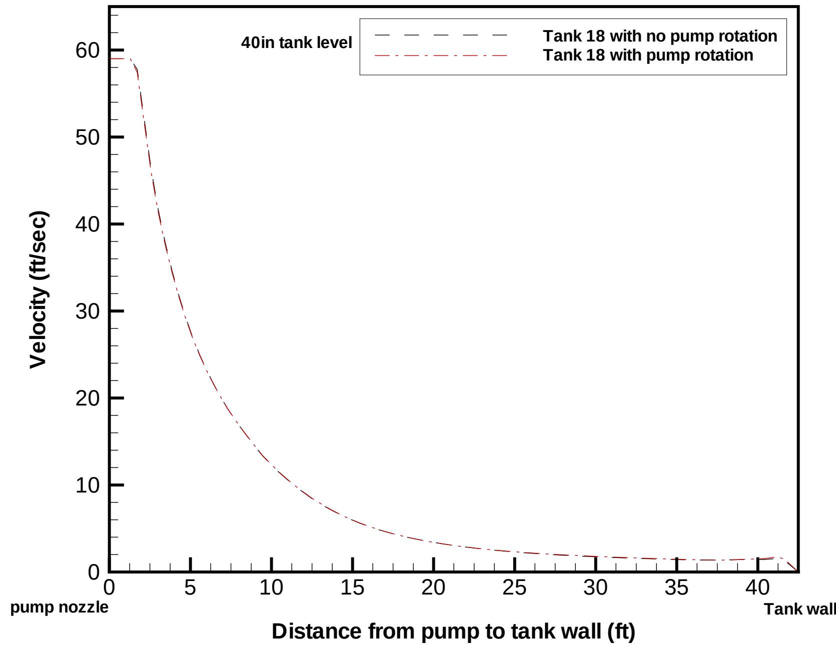

Figure 28. Downstream evolutions of Tank 18 with and without pump rotations for 40 in tank level at the discharge plane 27 inches above the tank bottom.

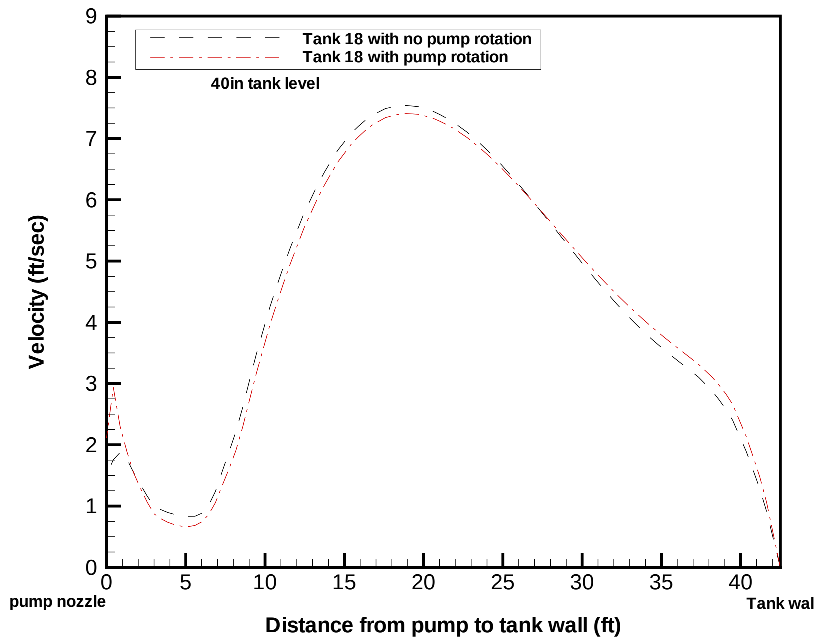

Figure 29. Downstream evolutions of Tank 18 with and without pump rotations for 40 in tank level at the discharge plane 3 inches above the tank bottom.

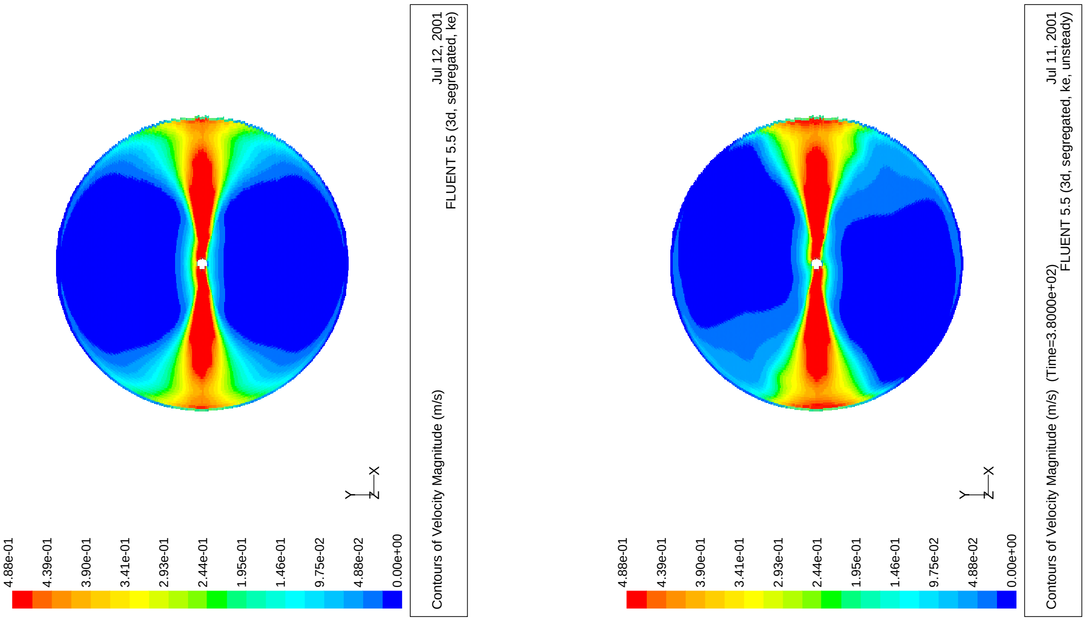

(no pump rotation for 40 in liquid level) (pump rotation for 40 in liquid level)

Figure 30. Steady-state downstream evolutions of Tank 18 with and without pump rotations for 40 in tank level at the discharge plane 27 inches above the tank bottom.

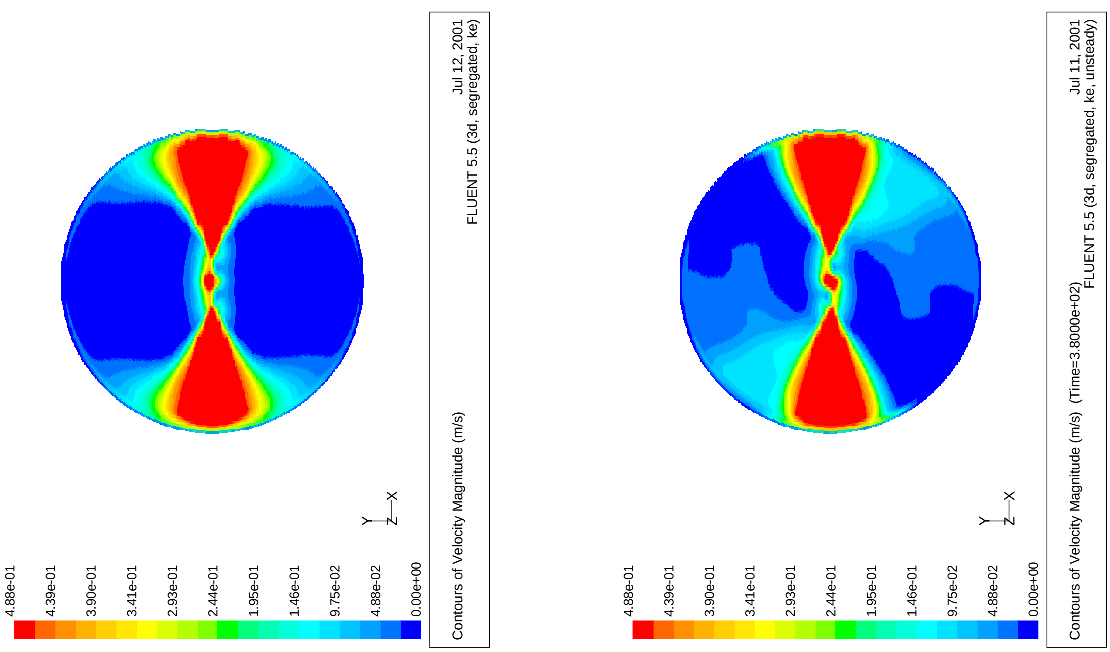

(no pump rotation for 40 in liquid level) (pump rotation for 40 in liquid level)

Figure 31. Steady-state downstream evolutions of Tank 18 with and without pump rotations for 40 in tank level at the discharge plane 3 inches above the tank bottom.

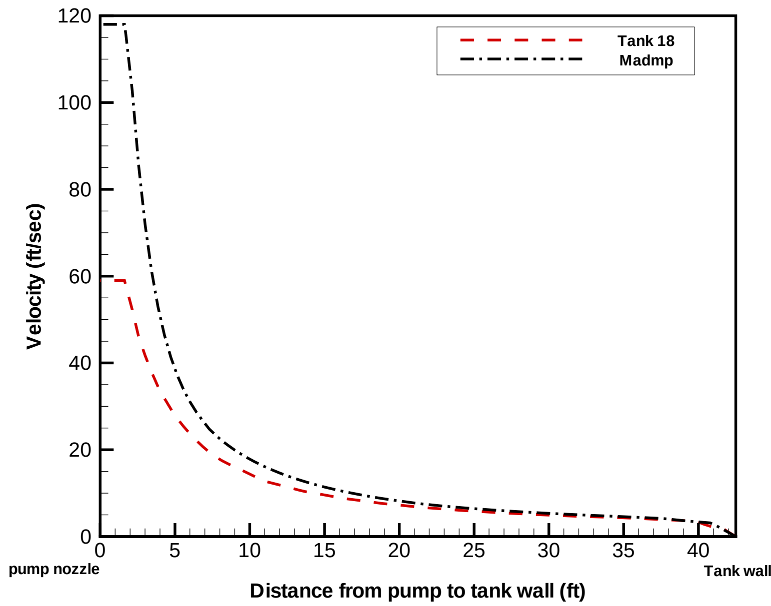

Figure 32. Downstream velocity profiles along the discharge directions of the nozzle planes of Tank 18 ADMP and MADMP mixers (The mapping name Tank 18 in the figure means Tank 18 operation with the existing ADMP.)

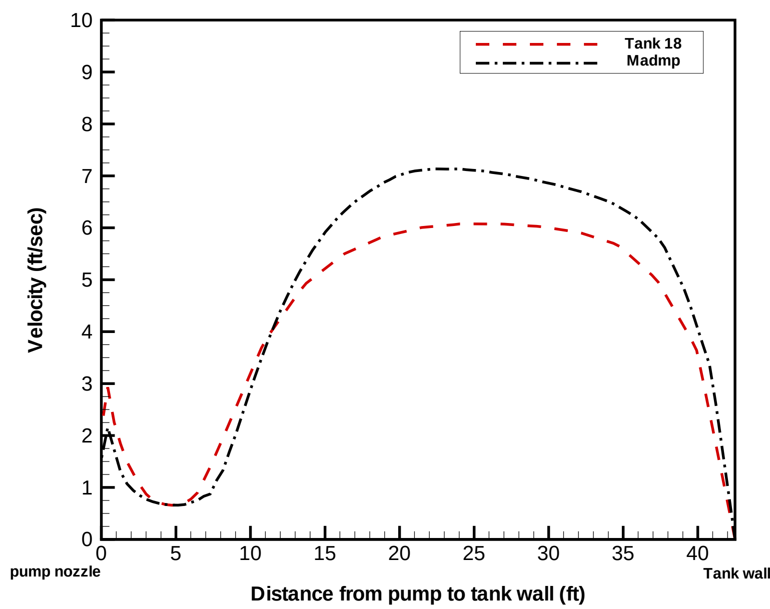

Figure 33. Horizontal velocity profiles along the downstream directions of the pump nozzles of Tank 18 with ADMP and MADMP mixers at the plane 3 in above the tank bottom (The mapping name Tank 18 in the figure means Tank 18 operation with the existing ADMP.)

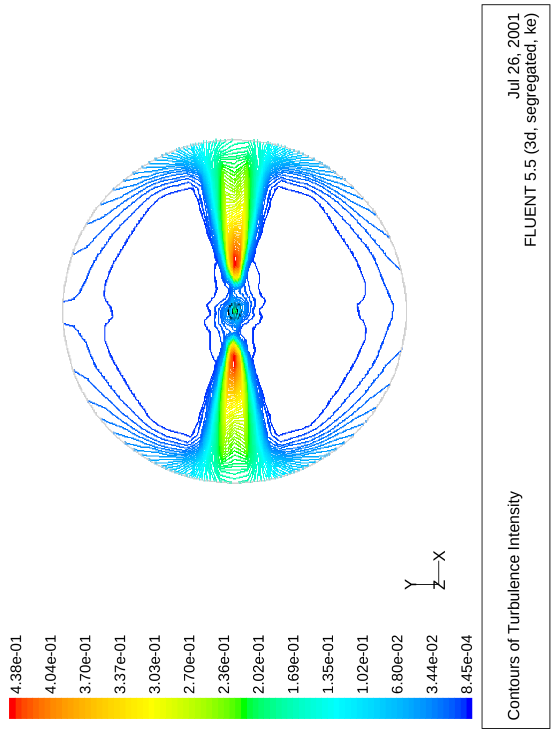

(Turbulence intensity contour plot for Tank 18 operation with ADMP mixer)

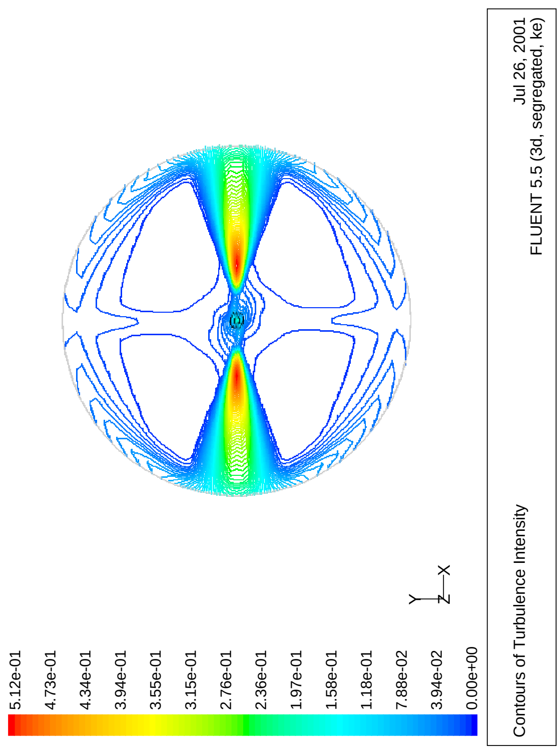

(Turbulence intensity contour plot for Tank 18 operation with MADMP mixer)

Figure 34. Comparison of turbulence intensity profiles for the Tank 18 operations with ADMP and MADMP mixers at the plane 3 in above the tank bottom

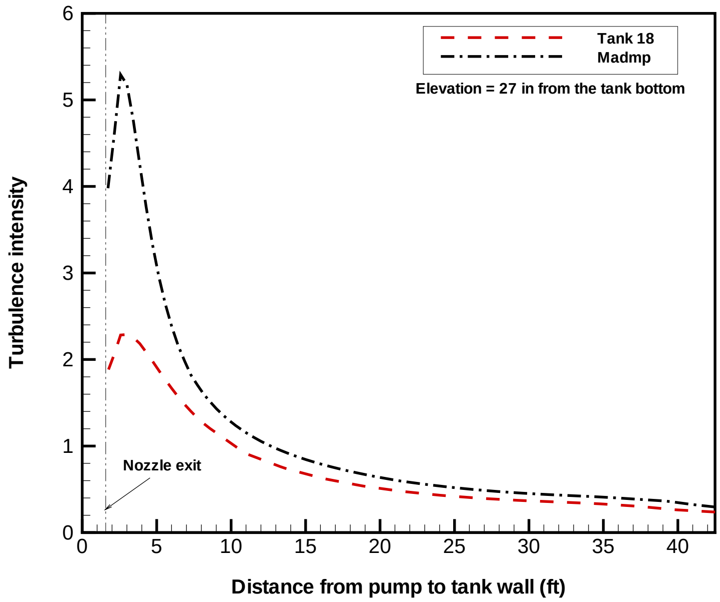

(Turbulence intensity profiles at 27 in elevation from the tank bottom)

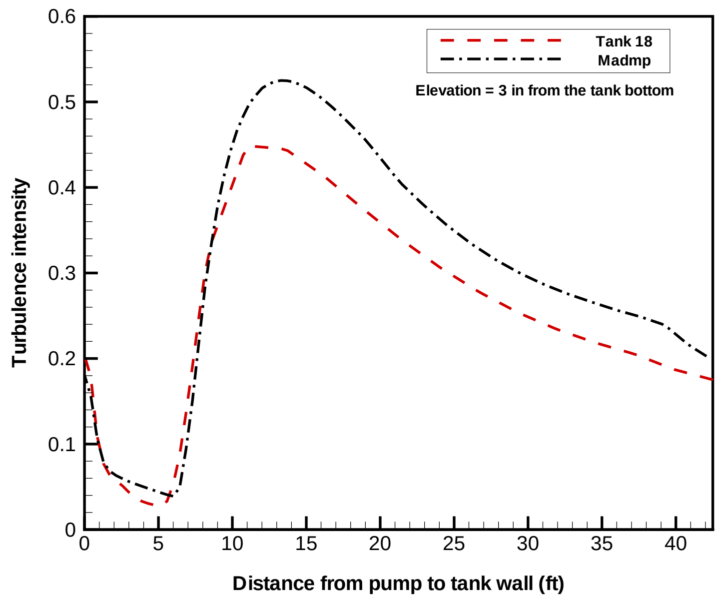

(Turbulence intensity profiles at 3 in elevation from the tank bottom)

Figure 35. Comparisons of turbulence intensity profiles for the Tank 18 operations with ADMP and MADMP mixers at the plane 3 in above the tank bottom (The mapping name Tank 18 in the figure means Tank 18 operation with the existing ADMP.)

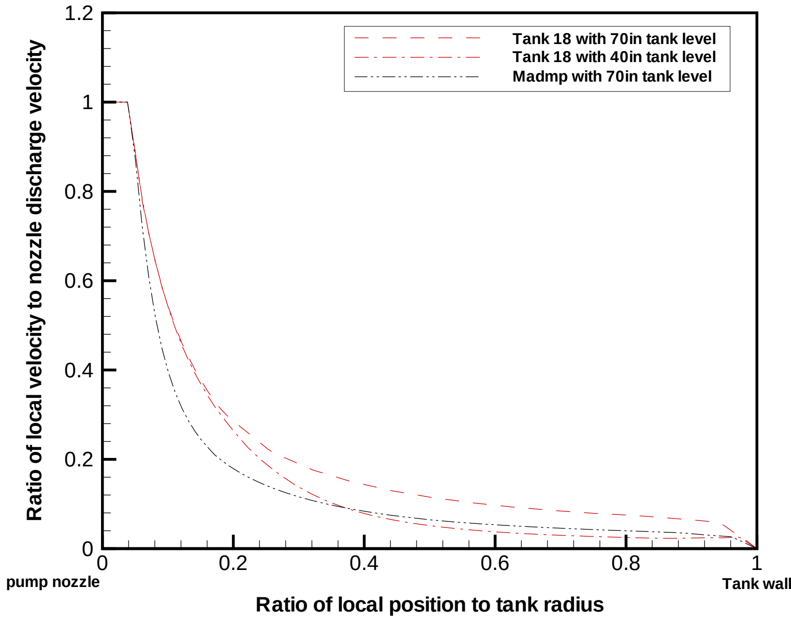

Figure 36. Nondimensional velocity distributions along the discharge direction of pump nozzle at the nozzle plane 27 in above the tank bottom (The mapping name Tank 18 in the figure means Tank 18 operation with the existing ADMP.)

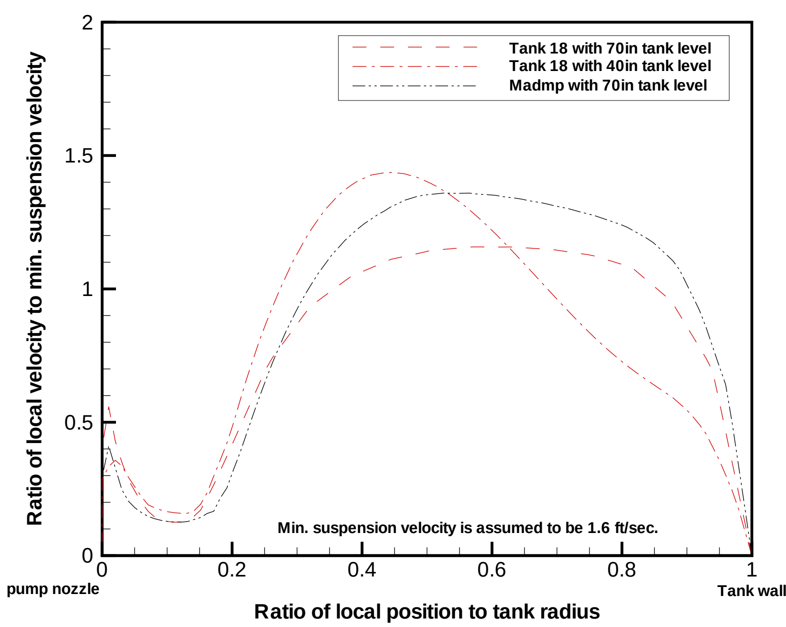

Figure 37. Nondimensional velocity distributions along the discharge direction of pump nozzle at the plane 3 in above the tank bottom (The mapping name Tank 18 in the figure means Tank 18 operation with the existing ADMP.)

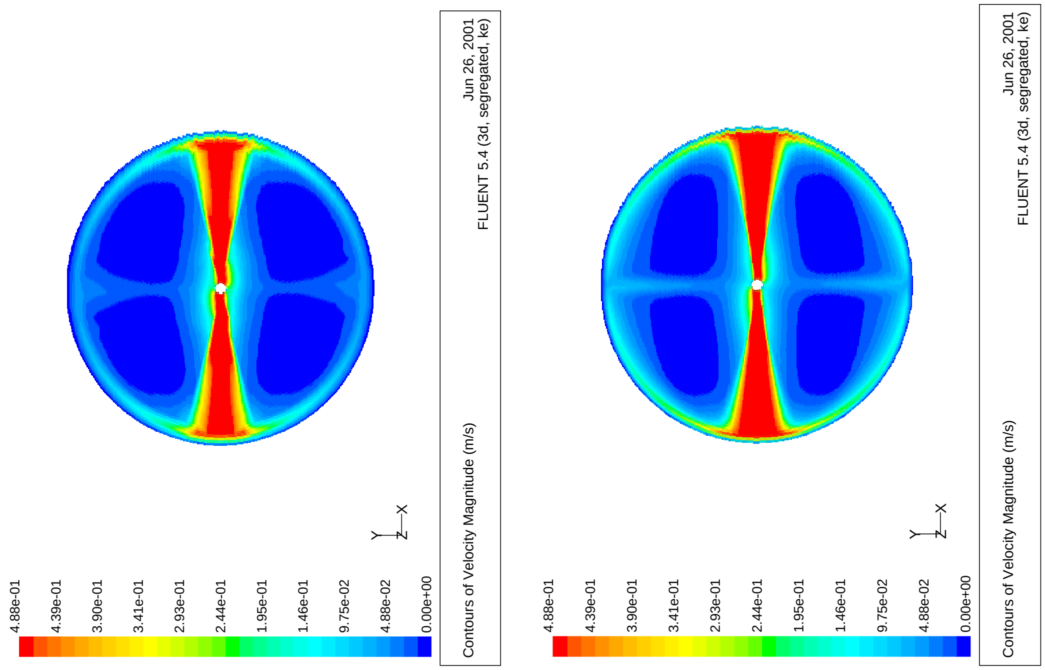

(Tank 18 with ADMP) (Tank 18 with MADMP)

Figure 38. Comparison of flow evolutions induced by the Tank 18 ADMP and MADMP mixers with 70 in tank levels on the discharge plane 27 in above the tank bottom

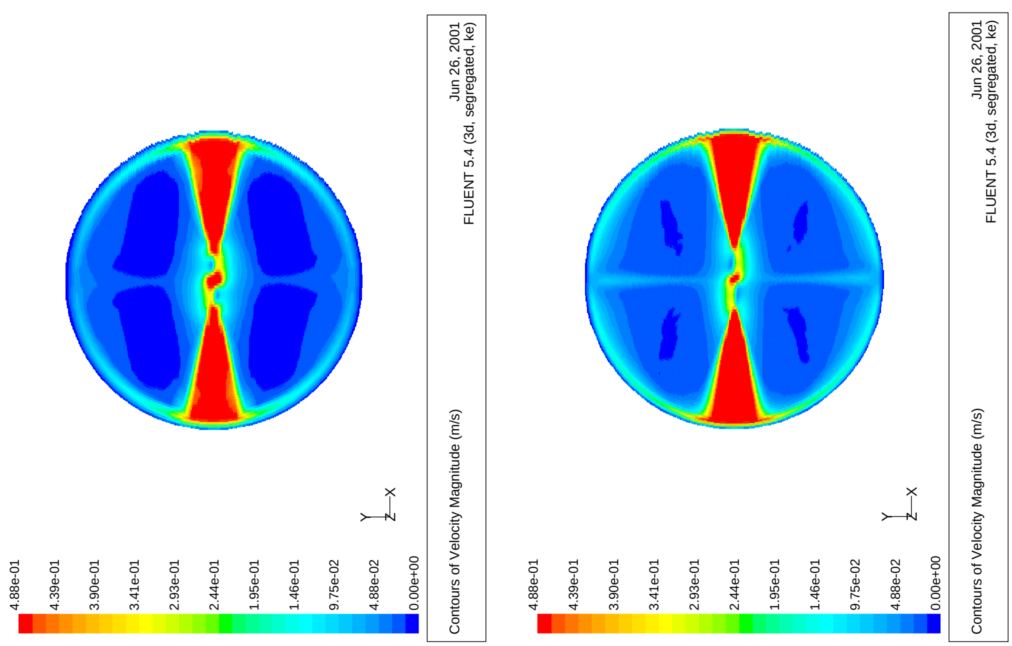

(Tank 18 with ADMP) (Tank 18 with MADMP)

Figure 39. Comparison of flow evolutions induced by the Tank 18 ADMP and MADMP mixers with 70 in tank levels on the horizontal plane 3 in above the tank bottom

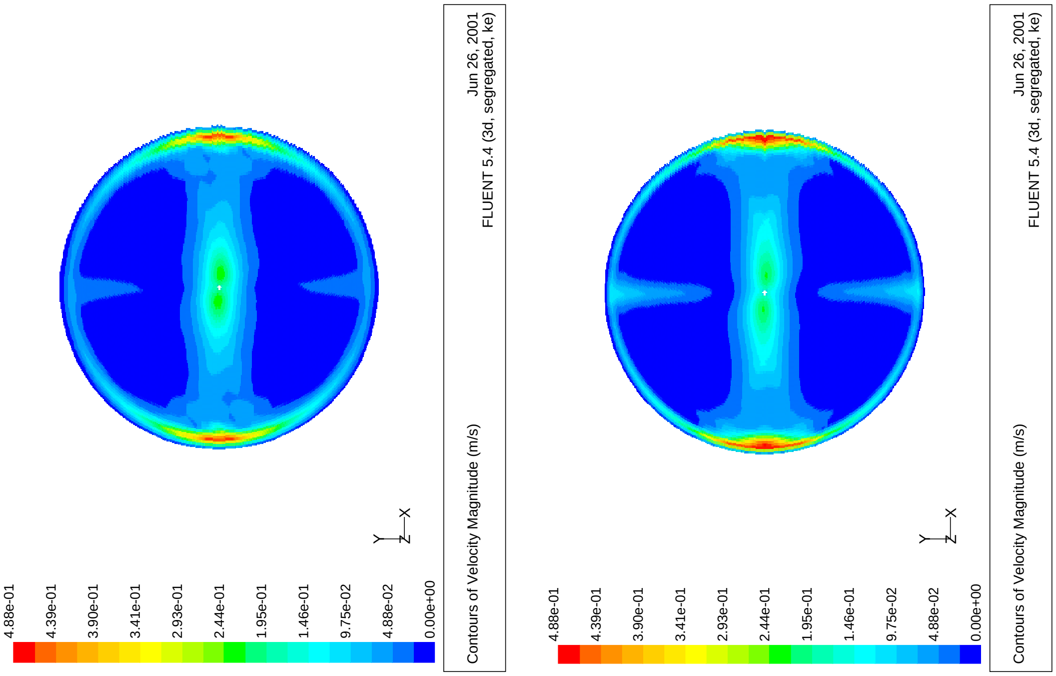

(Tank 18 with ADMP) (Tank 18 with MADMP)

Figure 40. Comparison of flow evolutions induced by the Tank 18 ADMP and MADMP mixers at the top surfaces of 70 in tank levels

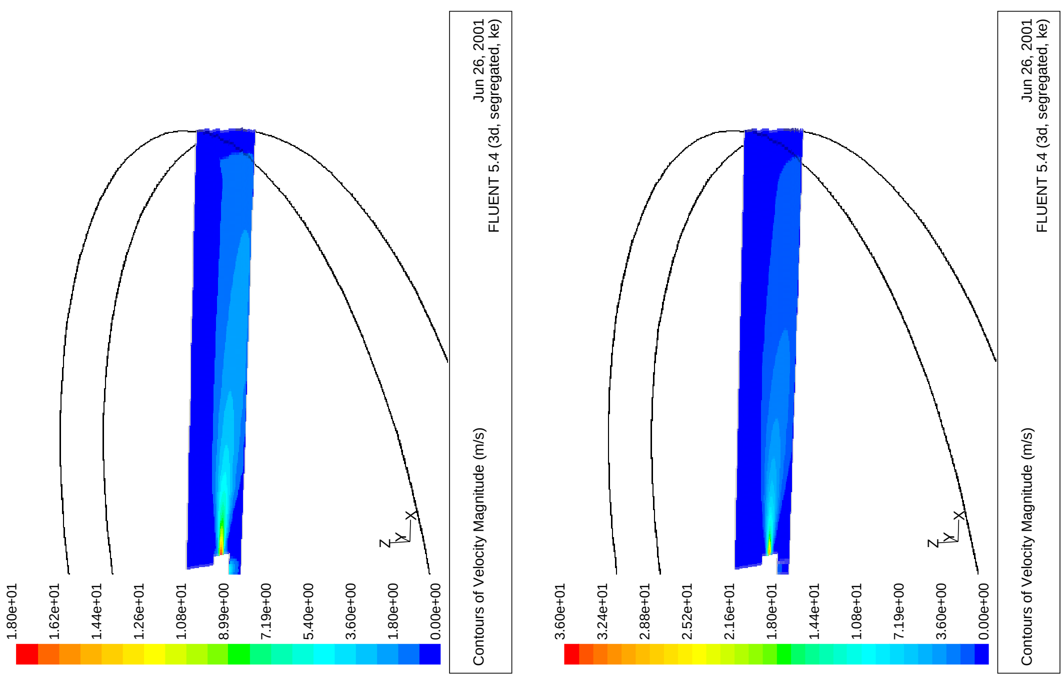

(Tank 18 with ADMP) (Tank 18 with MADMP)

Figure 41. Comparison of velocity contour plots induced by the Tank 18 ADMP and MADMP mixers at the center planes of 70 in tank levels

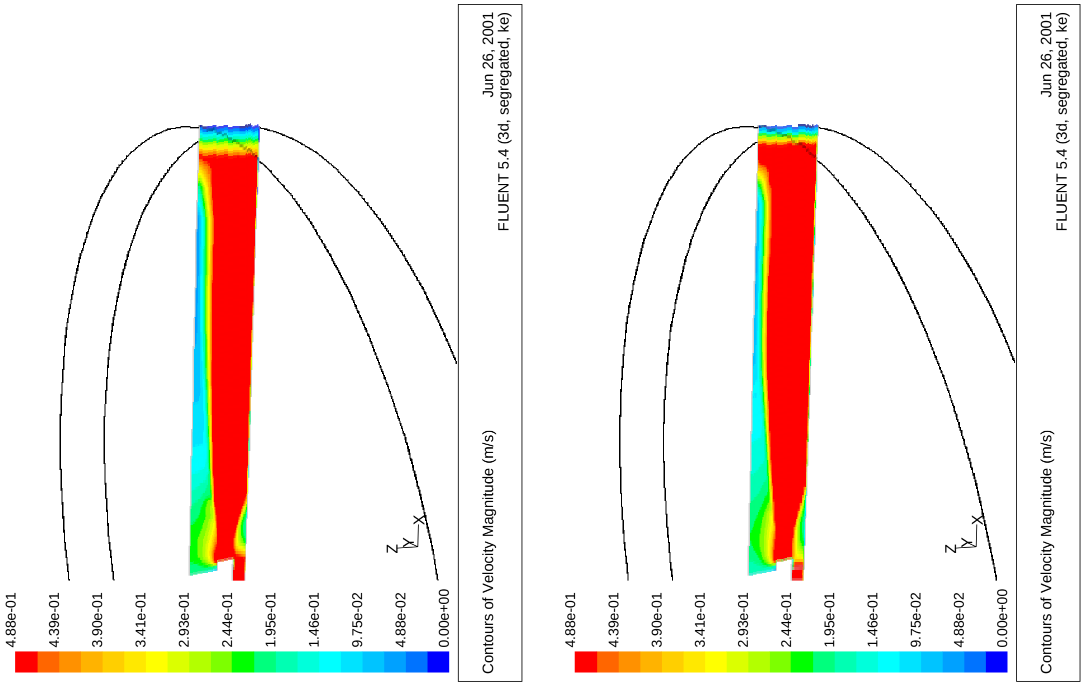

(Tank 18 with ADMP) (Tank 18 with MADMP)

Figure 42. Comparison of suspended zones of zeolites induced by the Tank 18 ADMP and MADMP mixers at the center planes of 70 in tank levels

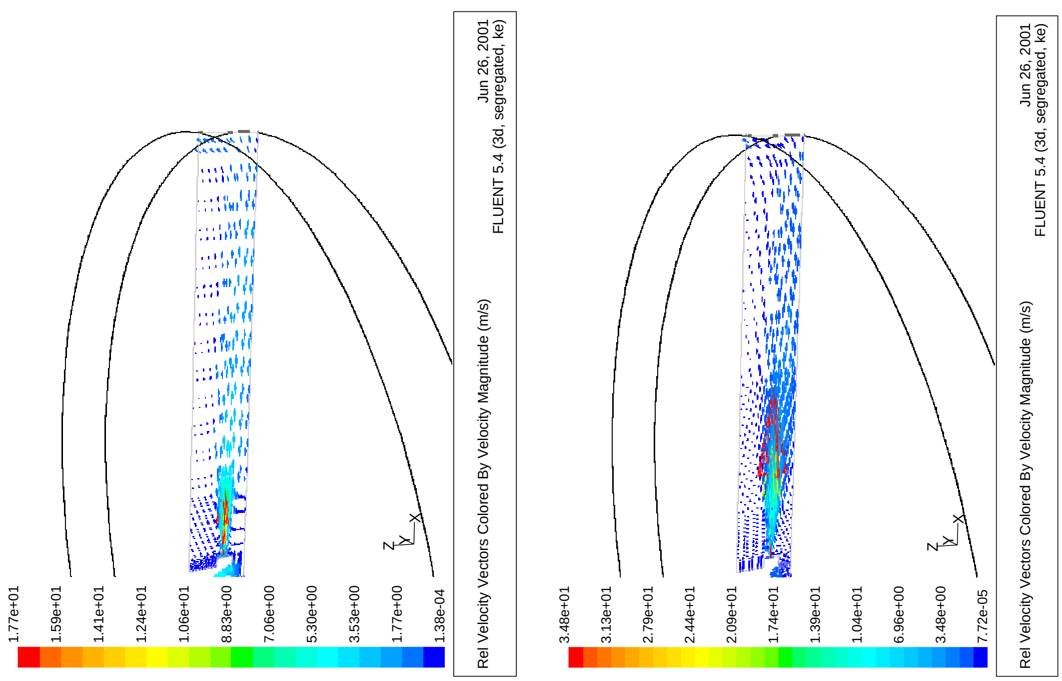

(Tank 18 with ADMP) (Tank 18 with MADMP)

Figure 43. Comparison of flow patterns induced by the Tank 18 ADMP and MADMP mixers at the center planes of 70 in tank levels

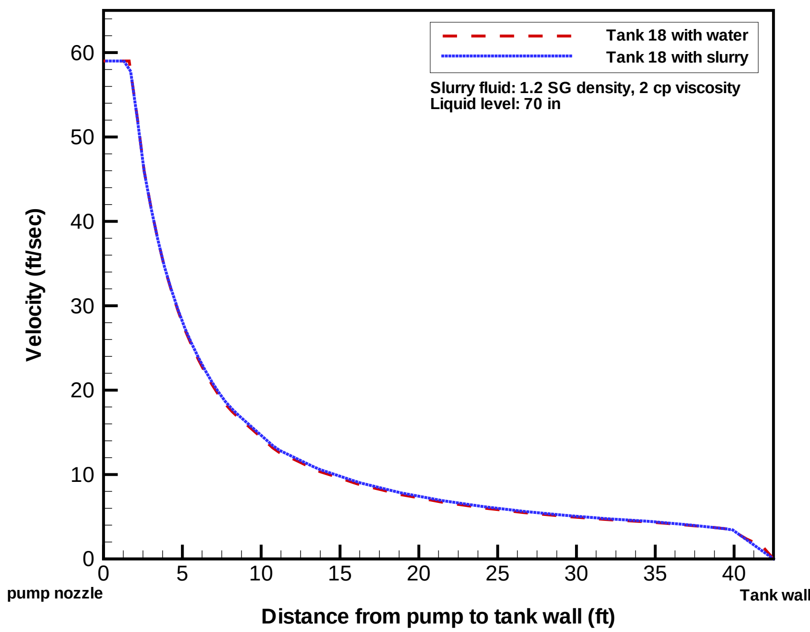

(velocity distributions at the level of nozzle exit)

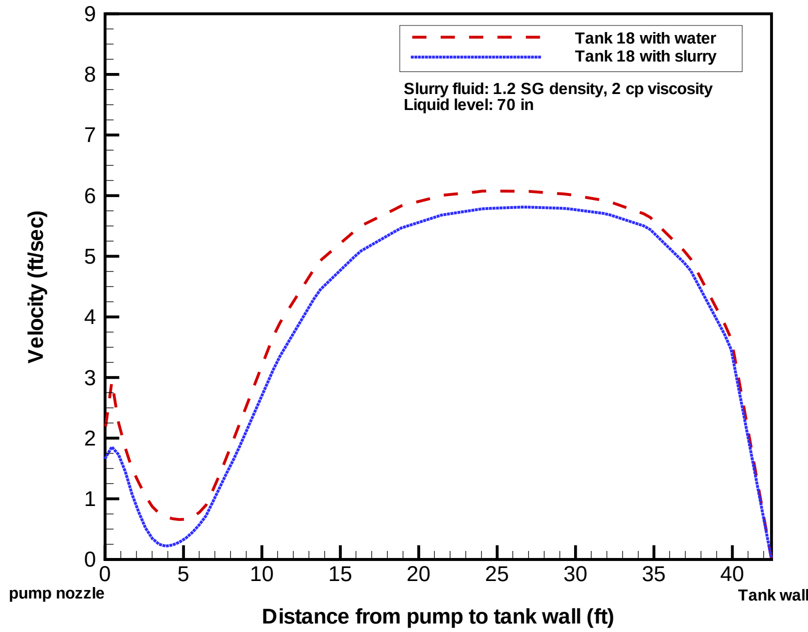

(velocity distributions at the 3 in elevation from the tank bottom)

Figure 44. Comparison of flow evolutions with two different mixing fluids induced by the Tank 18 ADMP mixer at the 27 in (nozzle exit level) and 3 in elevations from the tank bottom

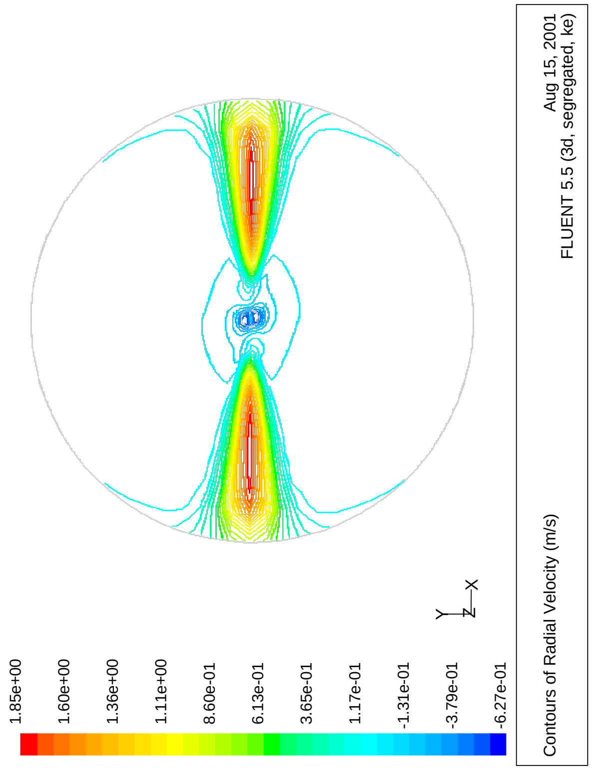

(Water flow evolutions at 3 in elevation from the tank bottom)

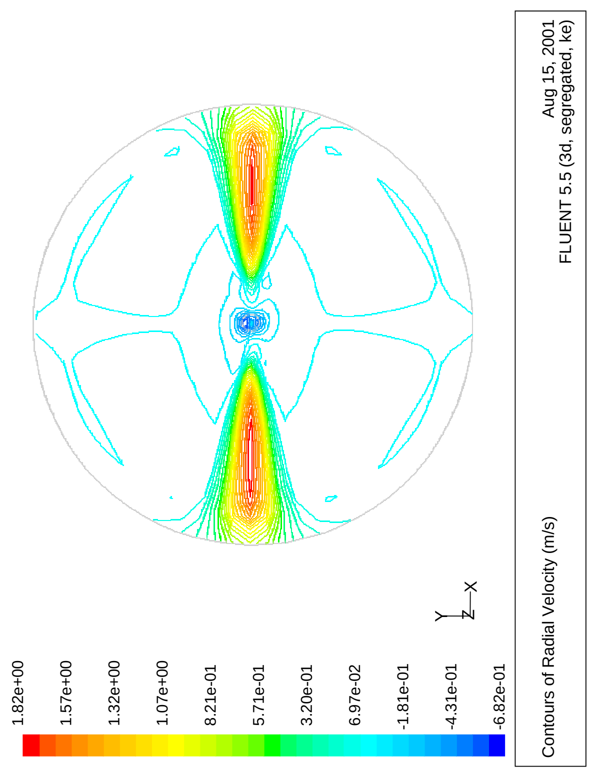

(Slurry flow evolutions at 3 in elevation from the tank bottom)

Figure 45. Comparison of flow evolutions with water and slurry fluids induced by the Tank 18 ADMP mixer at the 3 in elevations from the tank bottom

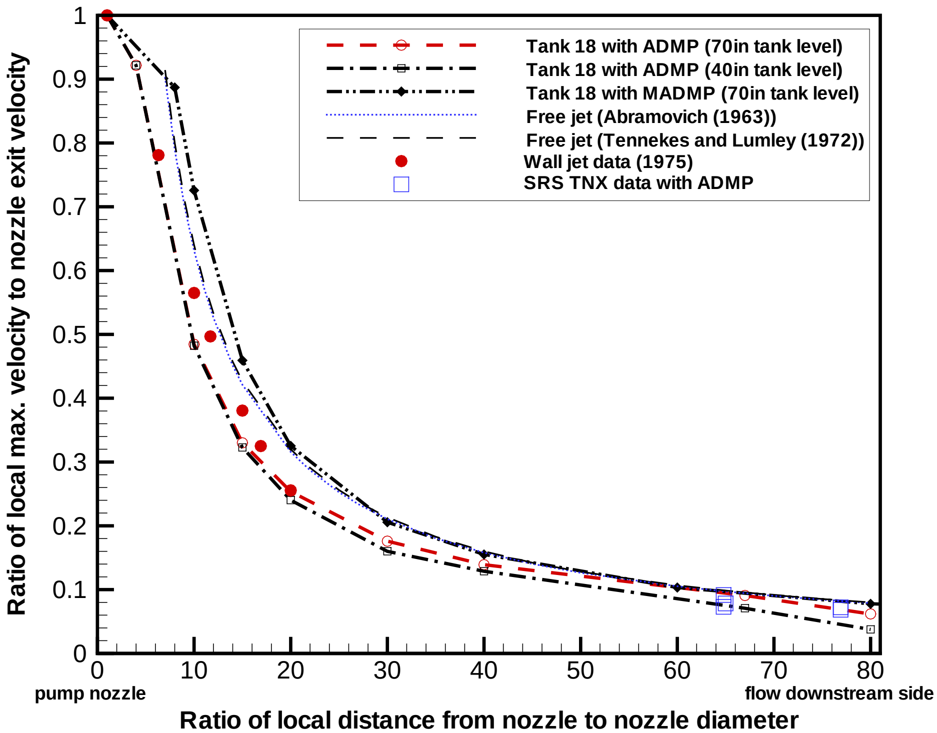

Figure 46. Comparisons of steady-state non-dimensional velocity profiles of Tank 18 at the discharge plane of ADMP mixer 27 in above tank bottom with literature data

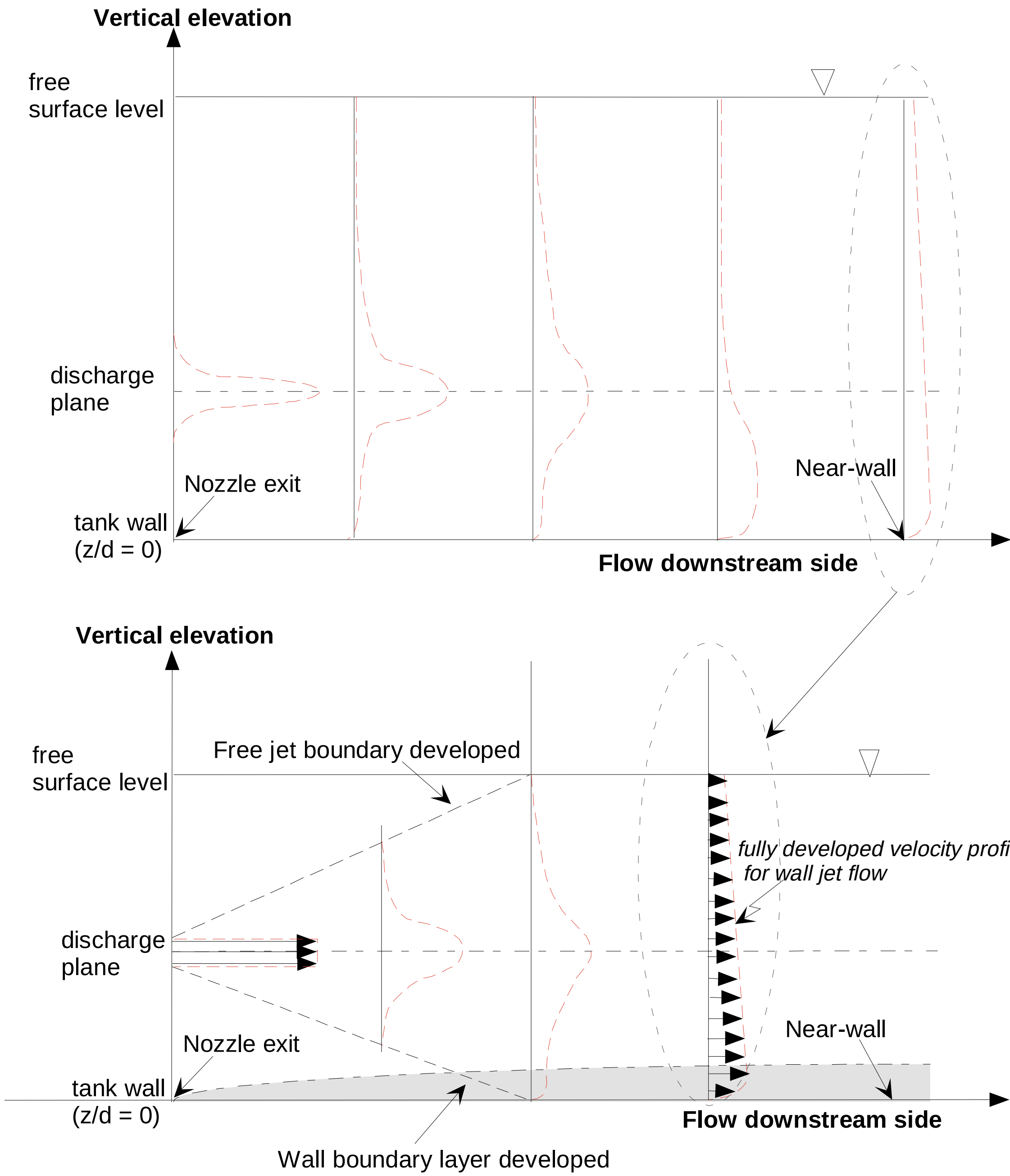

Figure 47. Typical velocity profiles in the direction perpendicular to the free surface from the modeling results of Tank 18 mixing simulations.

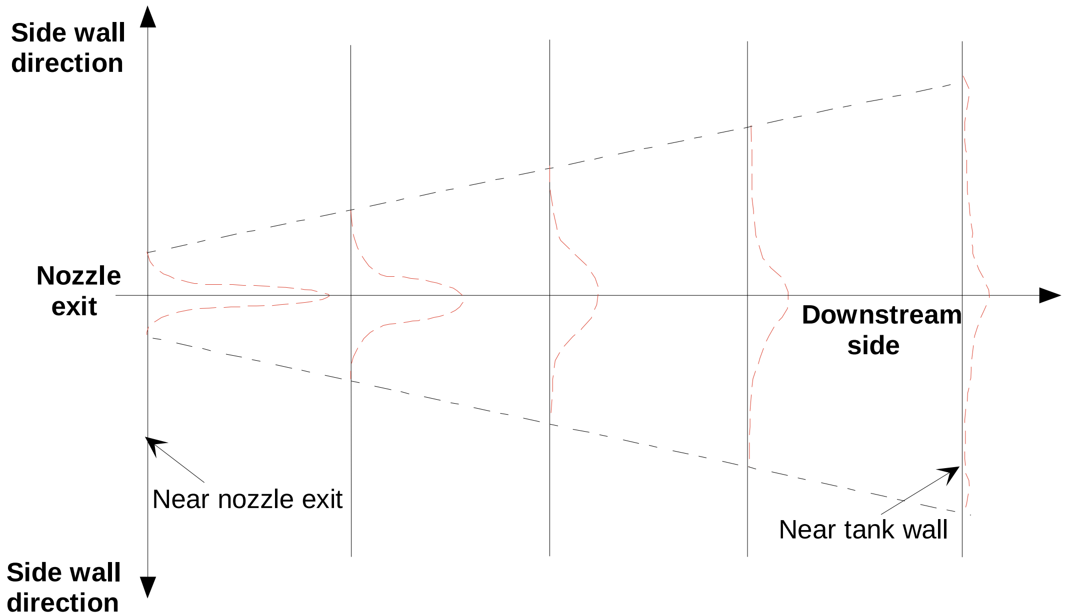

Figure 48. Typical velocity profiles in the direction parallel to the free surface from the modeling results of Tank 18 mixing simulations.

4. Summary and Conclusions

TNX full tank and Tank 18 simulation models with ADMP or MADMP mixers have been developed. Calculations have been performed to benchmark the models with TNX test data and to assess the efficiency of sludge suspension and removal operations in Tank 18 during steady-state and transient pump operations. Reference design and operating conditions were used as shown in Tables 3 and 4. Solid obstructions other than the pump housing and the 16" riser, and free surface motion of the tank liquid were neglected.

A three-dimensional analysis with a two-equation turbulence model was performed with FLUENT™, a commercial computational fluid dynamics (CFD) code. A two-dimensional approach was also used as a scoping analysis to examine multi-dimensional effects of fluid motion on the flow circulation pattern in the tank. The computed results were validated with TNX test and literature data. Rotational effects of the pump were considered to estimate the impact on the sludge suspension and removal assuming that local fluid velocity can be used as a measure of slurrying and mixing efficiency. For a minimum suspension velocity of 2.27 ft/sec, the results indicated that the existing ADMP mixer would provide adequate sludge removal from the tank with a 70 in liquid level except for a wall boundary of about 2 ft.

The CFD simulation results for the ADMP mixer showed that steady-state flow patterns were reached in about 60 seconds after starting the pump. As expected, the results also showed that when the pump was rotated in a continuous and one-way direction, the operational time to reach steady-state conditions was much longer. In addition, when the pump is off-center, times to reach steady-state flow patterns are much longer than the case with the pump located at the tank center.

The main conclusions are as follows:

- Model predictions agree with test data within about 25%. In the velocity ranges where sludge removal is required, the model provides a conservative estimate when compared to actual test data. The predictions are in good agreement with wall jet data available in the literature.
- The difference between a fixed pump and a rotating pump is small, and is well within the uncertainty of the present calculations. The pump with rotation appears to be somewhat better than the one with no rotation in terms of waste removal and suspension capabilities, largely because of secondary flows. The effect of pump rotation is more pronounced when the pump is located off-center and the tank liquid level is lower.
- Higher tank level results in better performance for suspending and removing the sludge for the given design and operating conditions of Tank 18.
- A smaller nozzle size with an identical $U_o d_o$ has better performance for suspending and removing the sludge for the given design and operating conditions of Tank 18. The MADMP mixer has the best performance among the cases considered in terms of sludge removal capacity.
- The computational results for two different fluids, water and a typical slurry (1.2 specific gravity, 2 cp), show that the maximum clearing distance is not sensitive to the slurry fluid properties. Therefore, all the flow pattern results based on water are valid for slurry flow in Tank 18.
- The results indicate that local velocities adjacent to the tank wall are potentially lower than those needed to remove sludge. The velocities are high enough to indicate that suspended zeolite will probably be swept aside.
- An approximate comparison (Appendix B) of results and observations from Tank 8 to the Tank 18 calculations documented here indicates that about 2000 gallons of sludge and zeolite mixture might lie in the bottom corner of Tank 18 beyond the reach of the ADMP.

(This Page Intentionally Left Blank)

5. References

1. R. A. Leishear, e-mail on design information of ADMP (LPI#91370), April 23, 2001.
2. HLW Technical Request Form, HLE-TTR-2001-049, Rev. 1, May 29, 2001.
3. N. V. Chadrasekhara Swamy and P. Bandyopadhyay, "Mean and Turbulence Characteristics of Three-Dimensional Wall Jets", *Journal of Fluid Mechanics*, Vol. 71, Part 3, pp. 541-562 (1975).
4. *FLUENT*, Fluent, Inc. (1998).
5. F. A. Zenz and D. F. Othmer, *Fluidization and Fluid-Particle Systems*, Chapter 6, Reinhold Publishing Corppration, New York (1960).
6. S. Y. Lee and R. A. Dimenna, "Validation Analysis for the Calculation of a Turbulent Free Jet in water Using CFDS-FLOW3D and FLUENT (U)", WSRC-TR-95-0170 (May 1995).
7. C. K. Madina and L. P. Bernal of F, "Interaction of a Turbulent Round Jet with the Free surface", *Journal of Fluid Mechanics*, Vol. 261, pp. 305-332 (1994)
8. Personal Communications with R. A. Leishear, April 21, 2001
9. Abramovich, G. N., "*The Theory of Turbulent Jets*", The MIT Press, Cambridge, MA, 1963.
10. H. Schlichting, *Boundary Layer Theory*, McGraw-Hill Book Company, New York (1967).
11. Personal communications with Marsh-McBirney, Inc.,

    Company Address: 4539 Metropolitan Ct., Frederick, Maryland 21704, Phone Number: (800) 368-2723, Fax Number: (301) 874-2172

    e-mail: www.Marsh-McBirney.com
12. W. M. Rohsenow and H. Y. Choi, *Heat, Mass, and Momentum Transfer*, Prentice-Hall, Inc., New Jersey (1961).
13. H. Tennekes and J. L. Lumley, *A First Course in Turbulence*, The MIT Press, Cambridge, MA, 1972.
14. B. V. Churnetski, "Effective Cleaning Radius Studies", Memorandum, DPST-81-282, February 19, 1981.
15. J. H. Perry, *Chemical Engineers' Handbook*, Fourth Edition, McGraw-Hill Book Co, New York.
16. E. J. Freed and O. S. Mukherjee, "Tank 8 Waste Removal Operating Plan", U-ESR-F-00009, Rev. 5, April 3, 2001.

(This Page Intentionally Left Blank)

Appendix A: Mapping of Velocity Measurement Sensor and Benchmarking Results

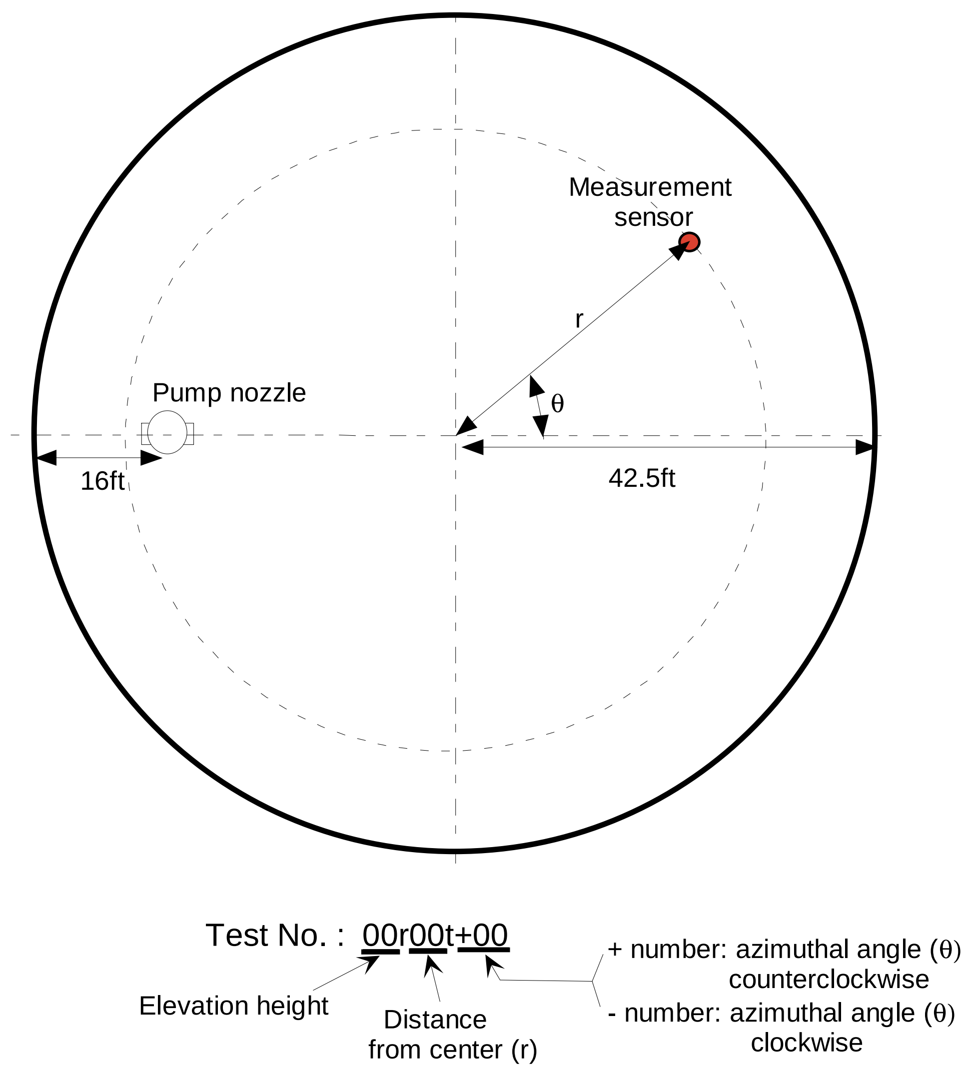

Figure A.1. Mapping of velocity measurement sensor for the TNX full tank test and notations of test number I.D. used in Table A.1.

Table A.1. Benchmarking results for TNX test with 3” and 27” elevations from the tank bottom

Test No.	Predictions	Experiments	% error
03r06t-23.7	4.800	4.715	1.8
03r06t-31.8	4.167	4.859	-14.2
03r12t-18.24	3.806	4.157	-8.4
03r12t-26.34	2.725	3.950	-31.0
03r18t-18.24	2.756	3.341	-17.5
03r18t-24.58	2.620	3.507	-25.3
03r24t-15.59	2.328	3.098	-24.8
03r24t-23.69	1.444	1.853	-22.1
03r30t-15.05	1.895	1.734	9.3
03r30t-23.15	1.142	1.260	-9.4
03r36t-14.66	1.499	1.483	1.1
03r36t-22.76	0.975	1.337	-27.1
03r42t-14.66	0.787	1.032	-23.7
27r12t+5.34	3.629	4.260	-14.8
27r06t+10.8	4.380	4.302	1.8
27r06t+15.9	4.100	2.840	44.4
27r06t+16.8	4.000	3.108	28.7
27r06t-10.8	4.380	5.402	-18.9
27r06t-5.34	4.590	4.623	-0.7
27r06t-23.7	3.644	3.811	-4.4
27r06t-31.8	3.280	4.085	-19.7
27r06t+97.7	0.720	1.858	-61.2
27r12t+11.34	3.270	2.530	29.3
27r12t+19.44	2.526	2.126	18.8
27r12t-18.24	3.100	4.033	-23.1
27r12t-26.34	2.210	3.445	-35.8
27r12t-5.34	3.629	4.036	-10.1
27r12t+92.24	0.100	1.444	-93.1
27r18t-3.58	3.031	3.137	-3.4
27r18t-24.58	1.478	2.642	-44.1
27r18t-16.48	2.223	3.180	-30.1
27r18t+11.34	2.450	1.745	40.4
27r18t+17.68	1.911	1.010	89.2

Table A.1. Benchmarking results for TNX test with 3" and 27" elevations from the tank bottom (continued)

Test No.	Predictions	Experiments	% error
27r18t+3.58	3.031	3.659	-17.2
27r24t-2.69	2.559	2.031	26.0
27r24t+2.69	2.559	2.378	7.6
27r24t+16.79	1.558	1.154	35.0
27r24t+8.69	2.198	2.009	9.4
27r24t-15.59	1.773	2.375	-25.3
27r24t+89.59	1.043	1.536	-32.1
27r30t-2.15	2.004	1.647	21.6
27r30t+2.15	2.004	1.587	26.2
27r30t+8.69	1.750	1.683	4.0
27r30t+16.25	1.173	1.045	12.3
27r30t+89.05	0.719	0.895	-19.6
27r30t-23.15	0.853	2.172	-60.7
27r30t-15.05	1.478	1.894	-22.0
27r36t-1.79	1.781	2.292	-22.3
27r36t+1.76	1.781	1.487	19.7
27r36t+15.86	1.299	1.875	-30.7
27r36t+7.76	1.519	1.489	2.0
27r36t-14.66	1.181	1.172	0.8
27r36t+88.66	0.981	1.256	-21.9
27r36t+22.76	0.822	1.349	-39.1
27r42t-1.53	0.924	1.145	-19.3
27r42t+1.53	0.924	1.110	-16.7
27r42t+7.76	0.904	2.204	-59.0
27r42t-14.43	0.989	1.592	-37.8
27r42t-22.56	0.591	0.660	-10.5
27r42t+42.63	0.554	0.585	-5.4
27r42t+69.53	0.984	0.917	7.3
27r42t+88.43	1.754	2.128	-17.6
27r42t+7.53	0.911	0.936	-2.7
27r42t+107.53	2.113	2.429	-13.0

(This Page Intentionally Left Blank)

Appendix B: Quantitative Estimation of the Remaining Sludge and Zeolite Volume

The flow patterns calculated in the Tank 18 analysis can be used to estimate the amount of sludge and zeolite that would be left behind because it is beyond the effective cleaning radius (ECR) of the pump. Observations and measurements from Tank 8 [Ref. 16] are used to quantify the ECR and calibrate the Tank 18 calculations.

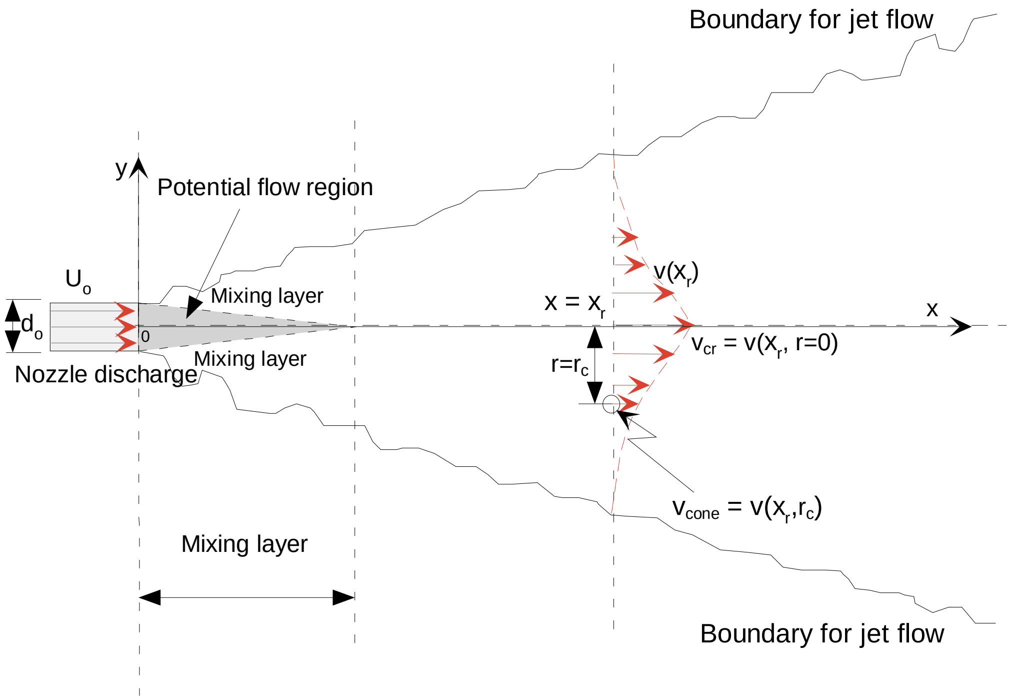

Figure B.1. Configuration of a turbulent free jet

A turbulent jet flow through a nozzle is dissipated as shown in Fig. B.1. The axial velocity distribution along the jet discharge line is described as follows:

$$v(x, r=0) = v_c(x) = K\left(\frac{U_o d_o}{x}\right) \qquad \text{(B1)}$$

Since the pump discharge flow is affected by the bottom of the tank, the constant *K* is evaluated from the Tank 18 calculations rather than classical free jet theory. It is found to be 4.874. The maximum axial velocity at any axial position x can be estimated using eq. (B1). The radial flow distribution v_r at a given axial position, $x = x_r$, is given in terms of radial position r perpendicular to the jet axis by the literature [Ref. 15].

$$log\left(\frac{v_{cr}}{v_r}\right) = K_r\left(\frac{r}{x_r}\right)^2 \qquad \text{(B2)}$$

Results from Tank 8 showed K_r to be 9.5 [Re. 16]. Then eq. (B2) becomes

$$log\left(\frac{v_{cr}}{v_{cone}}\right) = 9.5\left(\frac{r_c}{x_r}\right)^2 \quad \text{(B3)}$$

The ECR is defined as the distance from the nozzle exit to the point along the jet axis at which the local velocity is just equal to the minimum velocity needed to suspend sludge. This velocity is identified as v_{ECR}. This same magnitude of velocity can be found at an off-axis location and identified with v_{cone} as shown in Fig. B.1. Equating these two velocities and using eq. (B1) gives the suspension velocity,

$$v_{ECR} = v_{cone} = K\left(\frac{U_o d_o}{ECR}\right). \quad \text{(B4)}$$

From eqs. (B1) and (B4), the ratio of the axial velocity v_{cr} at $x = x_r$ to the ECR velocity v_{ECR} can be found.

$$\left(\frac{v_{cr}}{v_{ECR}}\right) = \left(\frac{v_{cr}}{v_{cone}}\right) = \left(\frac{ECR}{x_r}\right). \quad \text{(B5)}$$

From eqs. (B3) and (B5), the velocity terms can be eliminated. That is,

$$log\left(\frac{ECR}{x_r}\right) = 9.5\left(\frac{r_c}{x_r}\right)^2 \quad \text{(B6)}$$

Eq. (B6) can be used to relate two measured values from the Tank 8 report [Ref. 16], the disturbance depth r_c and the ECR. The disturbance depth is the depth to which the sludge layer was eroded by the horizontal jet. When these values are inserted in eq. (B6), the axial location x_r where the sludge is suspended and removed from the sludge hill can be calculated. The Tank 8 report lists the ECR and the disturbance depth r_c as 26 ft and 28 in, respectively, which gives a value x_r = 18 ft.

The sludge suspension velocity can be found from eq. (B5) if the axial velocity at x_r is known. The axial velocity at the 18 ft distance is given by eq. (B1). The discharge velocity at the Tank 8 jet nozzle was found to be 96.77 ft/sec for a 533 gpm flowrate (1600 rpm) and a 1.5 in nozzle diameter. Thus, the suspension velocity of the sludge was found to be 2.27 ft/sec. This value is consistent with the experimental observations in Tank 8 [Ref. 16]. Using this suspension velocity of the sludge and the present results of the Tank 18 model, the volume of the remaining sludge near the wall of the Tank 18 can be estimated. This suspension velocity for the sludge in Tank 18 corresponds to an ECR of 41.3 ft, which is about 1.2 ft away from the tank wall.

Figures B.2 and B.3 can be used to estimate the amount of sludge and zeolite in Tank 18 that is beyond the reach of the slurry pump. An engineering estimate is that sludge material would accumulate at a slope of about 60^o in the bottom corner of the tank. Therefore, an ECR of 41.3 ft would result in an accumulation as shown in Fig. B.2. If zeolite were to accumulate independently, its slope would be smaller, about 45^o. However, it is unlikely that this independent accumulation would occur in Tank 18, and it is beyond the scope of the present analysis. The tank material is expected to be a mixture of both sludge and zeolite, so Fig. B.2 encompasses both materials. The volume of this region has been evaluated numerically and is approximately 2044 gal.

It is possible that if the pump were to remain in a fixed position for a long enough period of time, it would ultimately erode the sludge layer and remove more sludge than is indicated in Fig. B.2. There is SRS engineering experience to indicate that this erosion could occur, but it was neither addressed nor supported by the analysis in this report.

A further question was raised about the tendency of suspended zeolite to drop out of the liquid region as the jet dispersed into the low velocity regions of the tank. While it is anticipated that such would be the case, deposition of the fast settling zeolite on the tank floor is a time dependent process that was not modeled in the present work. Qualitatively, one would expect the zeolite to drop out rather quickly once the liquid velocity dropped below that required to maintain the suspension. This would probably be in the green regions fairly close to the tank wall shown in Figure 23. That is, the deposition would be expected to follow behind the rotational motion of the jet, leaving an annular ring in approximately the outer third of the tank. The particulate would remain there until the opposing jet passed over that same region.

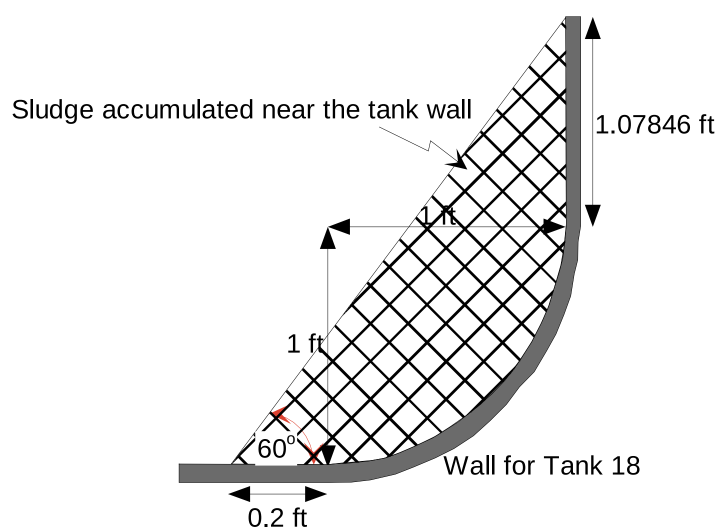

Figure B.2. Sludge mound remaining near the wall of Tank 18

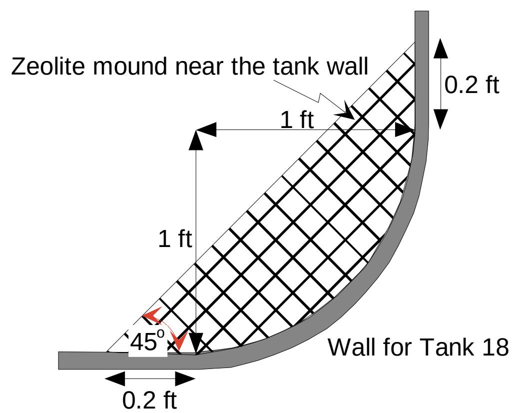

Figure B.3. Zeolite mound remaining near the wall of Tank 18